ACS APPLIED MATERIALS & INTERFACES

RESEARCH ARTICLE

www.acsami.org

Effect of Silica and Hydroxyapatite Mineralization on the Mechanical Properties and the Biocompatibility of Nanocomposite Collagen Scaffolds

S. Heinemann,* C. Heinemann, M. Jäger, J. Neunzehn, H. P. Wiesmann, and T. Hanke

Max Bergmann Center of Biomaterials and Institute of Materials Science, Technische Universität Dresden, Budapester Strasse 27, D-01069 Dresden, Germany

ABSTRACT: A recently established materials concept of biomimetic composites based on silica, collagen, and calcium phosphates was adapted for the preparation of porous scaffolds suitable for tissue engineering applications. Mineralization was achieved by directed nucleation of silica on the templating organic phase during a sol−gel process with or without addition of hydroxyapatite. Both mineral phases (25 wt %, individually or combined in equal shares) influenced the scaffold's morphology at the nanoscale. Enhancement of apparent density and compressive strength was similar for silica or hydroxyapatite mineralization; however the stiffening effect of hydroxyapatite was much higher. All scaffold modifications provided proper conditions for adhesion, proliferation, and osteogenic differentiation of human bone marrow stromal cells. The open porosity allowed cells to migrate throughout the scaffolds while maintaining their viability, both confirmed by MTT staining and confocal laser scanning microscopy. Initial cell distributions were graduated due to collagen mineralization, but balanced out over the cultivation time of 28 days. RT-PCR analyses revealed higher gene expression of ALP but lower expression of BSP II and osteocalcin because of collagen mineralization. The results demonstrate that both silica and hydroxyapatite offer comparable possibilities to tailor mechanical properties of collagen-based scaffolds without being detrimental to in vitro biocompatibility.

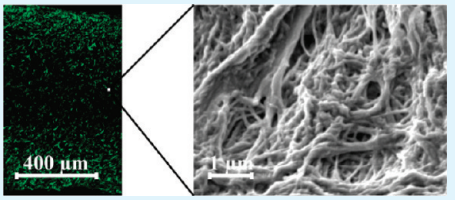

KEYWORDS: organic/inorganic composite, collagen scaffold, mechanical properties, human bone marrow stromal cell, osteoblast, biocompatibility, cell migration

1. INTRODUCTION

Three-dimensional scaffolds are required for structural support in order to regenerate lost bone. The pores of these scaffolds should be open and interconnected to allow cell growth, migration, and nutrient flow. During an intended implantation period the scaffold should degrade and be remodeled by osteoblasts and osteoclasts into native tissue.[1] Foamlike scaffolds are mostly obtained by removal of porogenes which allow to determine the pore size distribution.[2] Another type of three-dimensional scaffold is made by textile techniques that allow to process fibers into woven or nonwoven constructs.[3] When getting in contact with body fluids, sufficient and appropriate mechanical strength is required to maintain the three-dimensional architecture in order to facilitate cell culture tests in vitro, in vivo implantation, structural functionality once implanted, and biophysical stimuli to cells.[4]

Especially for the treatment of bone defects, biomaterials development recently focused on bioinspired or biomimetic materials and it has been recognized that the range of functionalities required cannot be covered by a monophasic material. Because bone is a natural composite built up from complexly structured mineralized collagen, artificial composites attracted increasing attention for the preparation of tissue engineering (TE) scaffolds. There is no general definition of the term composite; however, the following clarifications are commonly used in biomaterials research:[5,6] A composite is a multiphase material whose phases differ in composition and form. The phases retain their identities and properties, and are bonded, while an interface between them is maintained. A composite provides improved specific or synergistic characteristics not obtainable by any of the original phases alone. A composite becomes a nanocomposite when at least one of the components is of nanoscale size.[7] Decreasing the size leads to an increase in the surface and therefore to an enhanced cohesion between the components, mostly improving the mechanical properties.[8] In particular, organic/inorganic composites offer advantages; however, they also cause high complexity of the biomaterial/host tissue interaction.[9] Collagen is still established as a basic component of TE scaffolds because of inherent biocompatibility, biodegradability, osteoconductivity, and cost-effective availability. During a considerable number of studies, the formation of collagen/inorganic composites has been identified to be an option to overcome the drawback of insufficient stability. Most experience is gained for the combination of collagen with hydroxyapatite (HAp) leading to chemical compositions similar to that of natural bone.[10]

Furthermore, the combination of collagen and silica can be found in living nature as shown for marine glass sponges.[11] The role of silica in mammalian metabolism was intensively studied

Received: July 28, 2011
Accepted: September 26, 2011
Published: September 26, 2011

by Carlisle,[12] Schwarz,[13] and Seaborn.[14] They discovered that decrease in the silica level below critical values causes significant bone and cartilage diseases.

Silica and bioactive glasses composed of a silica network which is modified by alkaline oxides are biocompatible materials, which have become an interesting alternative or supplement to calcium phosphate based materials.[15,16] To achieve an intimate interaction between the phases, the sol−gel technique was confirmed to be an appropriate method for the conjugation of inorganic materials with biological systems, because of the compatibility of experimental conditions.[17] Gelatin, alginate, cellulose, chitosan, and collagen have been reported as biopolymer components in combination with silica.[18−20] The reactivity is generally based on the electrostatic interaction of the negatively charged silica species and positively charged groups of the organic component (e.g., amine groups of collagen) at neutral or near-neutral pH values.

In previous studies, the combination of collagen, silica, and calcium phosphates was already qualified for monolithic xerogels suitable for load-bearing bone substitution applications.[21,22] In the present study we adapted the processing strategy in order to obtain mechanically stable and biodegradable scaffolds which allow cell ingrowth. We used the sol−gel method to form nanosized silica particles on the surface of collagen and, furthermore, used nanosized HAp particles as the third component. The weight ratio of the three components was varied in order to tailor mechanical properties that were characterized by means of compressive tests in dry and wet state as well as chemically cross-linked. Scanning electron microscopy (SEM) was used to characterize the structure of the scaffolds and the influence of the mineral phases. Cell culture experiments were performed using human bone marrow stromal cells (hBMSC). The migration of the cells into the porous scaffolds was studied by means of both a macroscopic approach using MTT staining and a microscopic approach using actin staining recorded by confocal laser scanning microscopy (cLSM).

2. MATERIALS AND METHODS

2.1. Scaffold Preparation. Tetraethoxysilane (TEOS, 99%; Sigma, Taufkirchen, Germany) was hydrolyzed for 24 h at 4 °C by adding deionized water (molar ratio TEOS:water = 1:4) and hydrochloric acid (0.01 M HCl) as a catalyst. Orthosilicic acid ($Si(OH)_4$) obtained by this method served as the silica source. Bovine tropocollagen type I (GfN, Wald-Michelbach, Germany) was purified by salt precipitation (1 M NaCl) followed by dialysis against deionized water and mixed with 60 mM phosphate buffer at pH 7.4 and 37 °C in order to undergo fibrillogenesis.[23] Collagen fibrils were extracted and resuspended at a concentration of 20 mg/mL in 0.01 M Tris/HCl buffer pH 7.4. HAp (No. 102143; Merck, Darmstadt, Germany) was added as a powder to collagen suspensions and homogeneously stirred in.

Final collagen/silica/HAp mass percentages were 100/0/0 (C), 75/25/0 (CS), 75/0/25 (CH), and 75/12.5/12.5 (CSH). Total volumes of up to 2400 μL were chosen for the preparation of scaffolds for SEM, compressive strength tests, and cell culture experiments. Collagen or collagen-HAp suspensions were transferred to molds and silicic acid was added. After vigorous vortexing the samples were frozen at a cooling rate of 0.5 K/min to −20 °C in a SH-221 climate chamber (Espec, Osaka, Japan) followed by freeze-drying (Christ Alpha 1−4 lab freeze-dryer, Osterode, Germany). The scaffolds were chemically cross-linked by immersing in 1 wt % N-(3-dimethylaminopropyl)-N′-ethylcarbodiimide (EDC)/N-hydroxysuccinimide (NHS) (Sigma) in 40% ethanol for 24 h. Finally, the scaffolds were rinsed in deionized water and freeze-dried again. Samples designated for cell culture experiments were cut to 3 mm thick slices and gamma-sterilized at 25 kGy (Gammaservice, Radeberg, Germany).

2.2. Structural Analysis of the Scaffolds. Slices of fresh and cell-seeded scaffolds were mounted on stubs and coated with carbon. A high tension of 3 kV was applied in an ESEM XL 30 scanning electron microscope (Philips) working in high-vacuum mode and detecting secondary electrons for imaging. Especially cell-seeded scaffolds were critical point dried in liquid carbon dioxide after dehydration by immersion in graded series of ethanol/water.

For light microscopy imaging the scaffolds were fixed in 0.1 M phosphate buffer containing 2.5% glutaraldehyde (Roth, Karlsruhe, Germany) and dehydrated in graded series of alcohol. Subsequently, the specimens were transferred over propylene oxide (Merck) into Araldite (Agar scientific, Essex, UK). After polymerization for 3 days at 60 °C the embedded scaffolds were cut into 1 μm semithin sections using an EM UC 6 microtome (Leica, Vienna, Austria), drawn up on microscope slides and stained with toluidine blue (Sigma). Light microscopy was carried out using a Nikon Mikrophot FXA and Nis-Elements D software.

2.3. Compressive Strength Test. Scaffolds (diameter: 10 mm; height/diameter ratio: 2/1) were tested under uniaxial compressive load using an Instron 5566 (Darmstadt, Germany) instrument with a 100 N load cell (Instron) by simultaneously determining force and corresponding length variation. The rate of strain was set by adjusting the cross-head speed to 2 mm/min until 50% compression ultimately. Stress−strain relationships were determined in dry and wet state for at least five samples per composition and condition. The wet samples were soaked in PBS for 24 h before testing. Apparent density of the scaffolds was calculated as the quotient of the weight and the cylindrical volume. Young's modulus was calculated from the slope of a linear fit to the elastic range of the stress−strain curve. For cyclic measurements, wet samples were compressed 50 times to half of their initial height by maintaining a cross-head speed of 0.3 mm/s.

2.4. Cell Culture Experiments. HBMSC isolated from bone marrow aspirate were kindly provided by Prof. Bornhäuser and co-workers, Medical Clinic I, Dresden University Hospital.[24] The cells were expanded in Dulbecco's modified Eagle's medium (DMEM), low glucose, supplemented with 10% fetal calf serum (FCS), 100 U/mL penicillin, and 100 μg/mL streptomycin in a humidified atmosphere at 37 °C and 7% CO_2. Cells in passage 5 were used for the experiments. Medium and all supplements were obtained from Biochrom (Berlin, Germany).

Sterilized scaffolds were placed in 48-well polystyrene tissue culture plates and soaked in cell culture medium for 24 h in order to prevent floating. After aspirating the medium, excess liquid from the pores was removed by placing the scaffolds on a sterile filter paper. The samples were placed again in 48-well polystyrene tissue culture plates and 50 000 cells suspended in 50 μL of cell culture medium were seeded on top of each sample. After 30 min of initial adhesion, 750 μL of cell culture medium containing 50 μM ascorbate (os-) was added to the well. From the third day, one fraction of the cells was osteogenically induced by additional supplementation of 10 nM dexamethasone, 3.5 mM β-glycerophosphate and 10 nM 1,25-dihydroxyvitamin D3 to the medium (os+). All media were changed twice weekly and the cell-seeded scaffolds were cultivated for up to 28 days.

On specific time points the medium was removed, three samples per condition were washed with PBS and frozen at −80 °C until biochemical analysis. Samples for microscopic analysis taken after 1, 14, and 28 days, were fixed with 3.7% formaldehyde in PBS and stored at 4 °C. After 28 days of cultivation six samples per composition were washed with PBS and used for RNA extraction followed by reverse transcriptase polymerase chain reaction (RT-PCR).

2.5. Biochemical Analysis. Frozen samples and 900 μL PBS were placed into precellys tubes (Peqlab, Erlangen, Germany) and crushed

Table 1. Primer Sequences Used for RT-PCR

gene	forward primer (5′-3′)	reverse primer (5′-3′)
GAPDH	GGTGAAGGTCGGAGTCAACGG	GGTCATGAGTCCTTCCACGAT
ALP	CACGGGCACCATGAAGGAAAA	ATTCTCTCGTTCACCGCCCAC
BSP II	AATGAAAACGAAGAAAGCGAAG	ATCATAGCCATCGTAGCCTTGT
OC	CAAAGGTGCAGCCTTTGTGTC	TCACAGTCCGGATTGAGCTCA

with steel balls for 20 s at 5900 rpm in a precellys homogenizator (Peqlab). For cell lysis, 100 μL of 10% Triton X-100 were added for 1 h on ice. Afterward the whole suspension was centrifuged at 10000 rpm for 30 s and the supernatant cell lysate was used for the following colorimetric measurements on a SpectraFluor Plus microplate reader (Tecan, Mainz-Kastel, Germany).

Cell proliferation was determined through the total activity of lactate dehydrogenase (LDH) using the LDH Cytotoxicity Detection Kit (Takara, Otsu, Shiga, Japan). An aliquot of cell lysate was mixed with LDH substrate buffer and the enzymatic reaction was stopped after 20 min with 0.5 M HCl. The absorbance was read at 492 nm. The LDH activity was correlated with the cell number using calibration lines of cell lysates with known cell numbers.

Cell differentiation was evaluated by the activity of alkaline phophatase (ALP). An aliquot of cell lysate was added to ALP substrate buffer, containing 2 mg/mL p-nitrophenyl phosphate (Sigma), 0.1 M diethanolamine, 1 mM $MgCl_2$, 0.1% Triton X-100 (ph 9.8) and the mixture was incubated at 37 °C for 30 min. The enzymatic reaction was stopped by the addition of 0.5 M NaOH and the absorbance was read at 405 nm. A calibration line was obtained from different concentrations of p-nitrophenol.

2.6. RT- PCR. Gene expression of the cells cultivated on the porous scaffolds was analyzed after 28 days. The peqGOLD MicroSpin Total RNA Kit (Peqlab) was used to isolate the RNA according to the manufacturer's instructions. RNA concentration was measured using a Nanodrop ND 1000 (Peqlab). For the transcription of cDNA, a 20 μL reaction mix containing 400 ng of total RNA, 200 U of Superscript II Reverse Transcriptase (Invitrogen, Darmstadt, Germany), 0.5 mM dNTP (Invitrogen), 12.5 ng/μL random hexamers (MWG Biotech, Ebersberg, Germany), and 40 U of RNase inhibitor RNase OUT (Invitrogen) was prepared and incubated for 50 min at 42 °C followed by 15 min at 70 °C in a Primus 25 Advanced thermocycler (Peqlab). PCR was performed using 2 μL of cDNA as a template and adding 18 μL of master mix containing specific primer pairs to detect the transcripts of alkaline phosphatise (ALP), bone sialoprotein II (BSP II), osteocalcin (OC), and the housekeeping gene GAPDH. Primer sequences are summarized in Table 1. After the initial activation step at 95 °C for 4 min, 25−35 PCR cycles were run with each a denaturation step at 95 °C for 45 s, an annealing step for 55 s, and a synthesis step at 72 °C for 1 min followed by a final synthesis step at 72 °C for 10 min. The same single-stranded cDNA was used to investigate the expression of the genes described. The resulting PCR products were analyzed using the Flash-Gel Dock and documentation system (Cambrex Bio Science, East Rutherford USA). Expression of the markers was normalized to the expression of GAPDH by image analysis using the BioImaging System Gene Genius with the acquisition software GeneSnap and the Gene-Tools software (SynGene, Cambridge, U.K.).

2.7. MTT Staining. After 1 day and 14 days of cultivation, cell-seeded scaffolds were immersed for 4 h in culture medium supplemented with 1.2 mM 3-(4,5-dimethylthiazol-2-yl)-2,5-diphenyltetrazolium bromide (MTT; Sigma). Staining by dark blue formazan derivative developed during 4 h of incubation at 37 °C and was documented using a digital camera (Canon).

2.8. Confocal Laser Scanning Microscopy. Cytoskeletal actin as well as the nuclei of the fixed cells was stained with AlexaFluor 488-Phalloidin (Invitrogen) and 4′,6-diamidino-2-phenylindole (DAPI, Sigma), respectively. Furthermore, ALP was stained after 14 days of cultivation using the ELF97 Endogenous Phosphatase Detection Kit (Invitrogen). Microscopy was carried out on an upright Axioscop 2 FS mot equipped with a LSM 510 META module (Zeiss, Jena, Germany). Excitation of AlexaFluor 488 was carried out at 488 nm with an Ar^+ laser. A NIR-femtosecond titanium-sapphire laser (Coherent Mira 900F, Santa Clara, CA, USA) was used at 750 nm 2-photon excitation to excite simultaneously fluorescence emission of DAPI detected at around 460 nm as well as ELF97 detected at around 530 nm. Both fluorescence emissions could be nearly entirely separated using the spectral sensitive Zeiss META detection system.

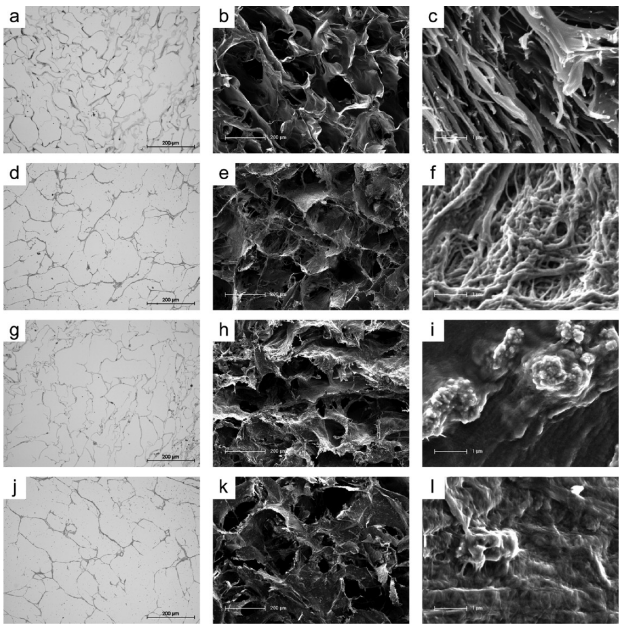

Figure 1. Light microscopy (first column) and SEM (second and third column) cross-sectional views of collagen-based scaffolds (a−c) without mineral phase (C), (d−f) with 25 wt % silica (CS), (g−i) with 25 wt % HAp (CH), and (j−l) with 12.5 wt % silica +12.5 wt % HAp (CSH), respectively.

2.9. Statistics. All measurements were collected at least in triplicate and expressed as mean ± standard deviation. One-way analysis of variance (ANOVA) was applied for statistical analysis and P values <0.05 were considered significant and indicated by one asterisk. Furthermore ** indicate $P < 0.01$, and *** $P < 0.001$.

3. RESULTS

3.1. Structure of the Scaffolds. Light microscopy and SEM was used to evaluate the microstructure as well as the nanostructure of the porous three-dimensional scaffolds. For all compositions − independent from mineralization − an open and interconnected porosity with pore sizes varying in the range of

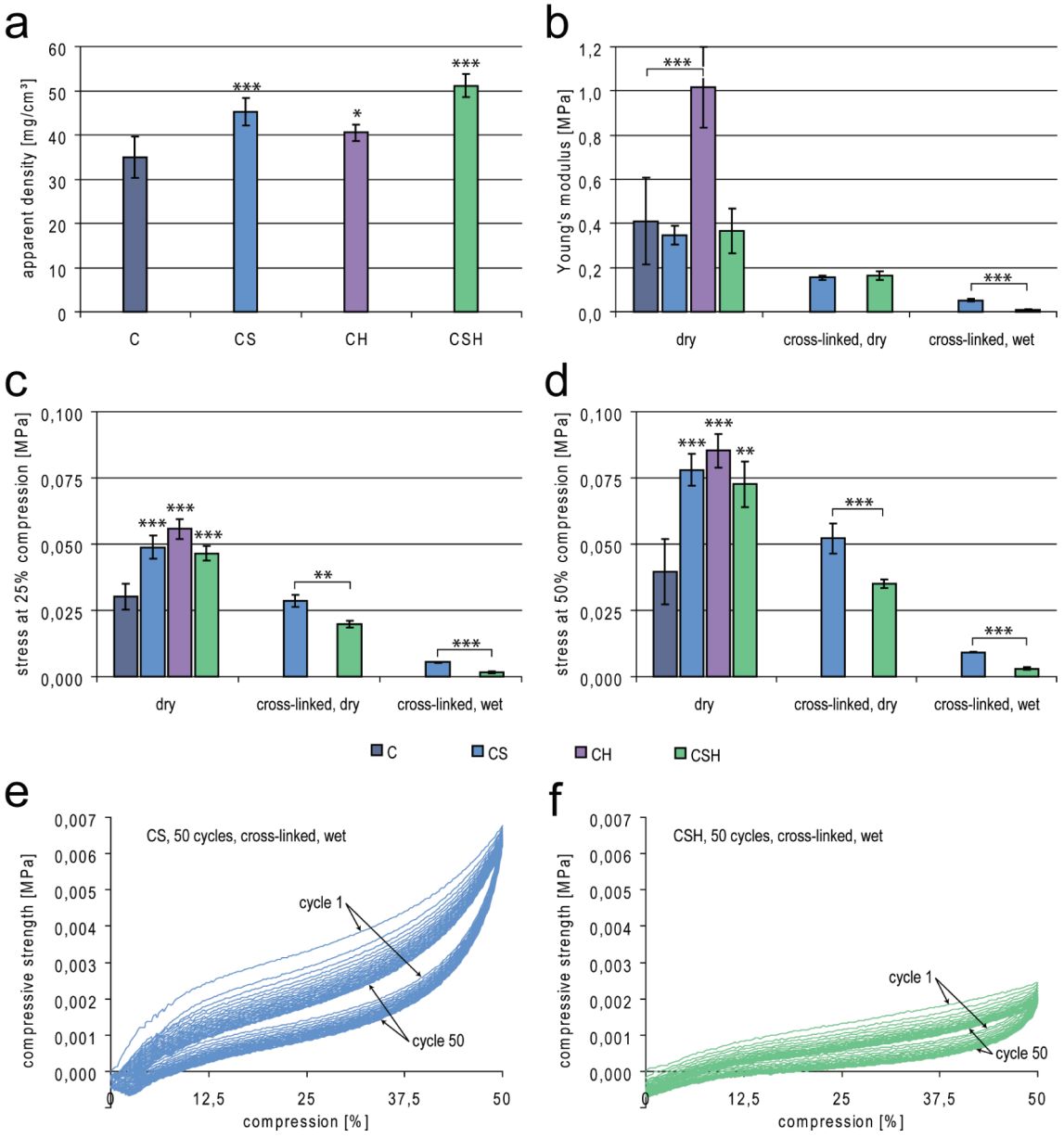

Figure 2. Apparent density, Young's modulus, and stress at 25% as well as 50% compression calculated for the collagen scaffolds without mineral (C), with 25% silica (CS), with 25% HAp (CH), and 12.5% silica +12.5% HAp (CSH), respectively. Cyclic measurements with cross-linked, wet CS and CSH samples were performed by applying 50 cycles of uniaxial compression at 0.3 mm/s.

100−200 μm was observed (Figure 1). However, the pore walls of the pure collagen scaffold were clearly smoother compared to that with mineral phases which obviously disturbed the formation process resulting in roughened surfaces. Clear influence of the mineral phases on the structure was detected at higher magnification. The pure collagen scaffold is build up from fused collagen fibrils (c), whereas the presence of silica prevents the lateral alignment of the collagen fibrils resulting in irregular oriented and separated fibrils (f). HAp is embedded as particles in the collagen matrix (i). The scaffold composed of collagen and both mineral phases (l) showed really a mixture of the morphological features recognized for (f) and (i).

3.2. Mechanical Properties. The apparent density of the scaffolds with mineral (CS, CH, CSH) was only slightly higher than that of the pure collagen scaffold (C) (Figure 2a). The density of samples with silica or silica+HAp was higher than with HAp alone. The Young's modulus of the dry and not chemically cross-linked collagen scaffolds was about 0.4 MPa and silica had no stiffening effect (Figure 2b). In contrast, mineralization with HAp resulted in enhancement of the modulus by a factor of about 3, but no stiffening effect was apparent for the three-component scaffold. The strength at 25% compression in the dry state increased about 1.5-fold due to the mineralizations and increased from 25 to 50% compression (Figure 2c, d). Absolute values for CS and CH scaffolds were similar over the whole compression range finally reaching about 0.085 MPa at 50% compression. When the same total percentage was applied by combining both mineral phases equally, compressive strength tended to decrease.

Soaking for chemical cross-linking caused deformation and shrinkage of the pure collagen scaffolds (C) as well as the

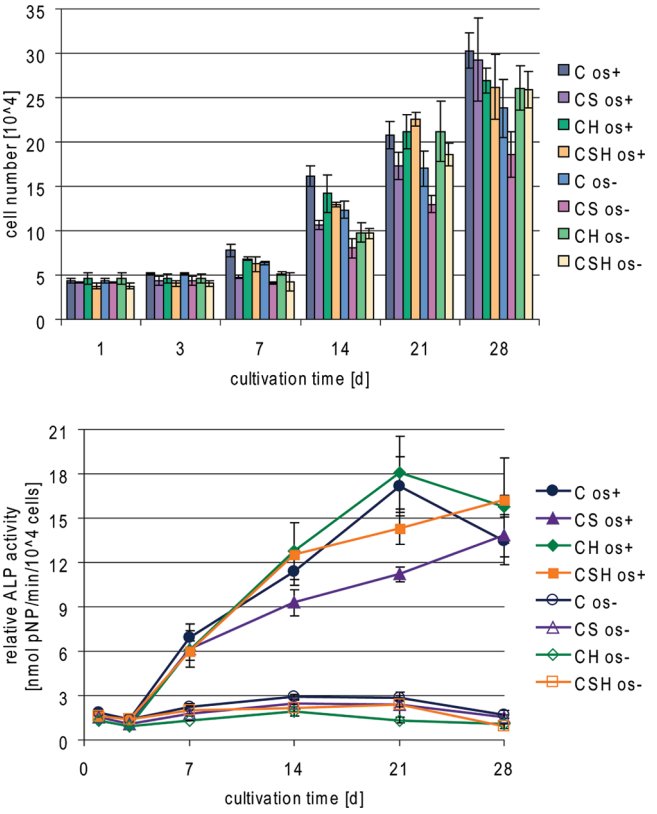

Figure 3. Proliferation and differentiation of hBMSC determined by LDH and relative ALP activity analysis. Cells were cultivated with osteogenic supplements (os+) or without osteogenic supplements (os−) on collagen scaffolds without mineral (C), with 25% silica (CS), with 25% HAp (CH), and 12.5% silica and 12.5% HAp (CSH), respectively.

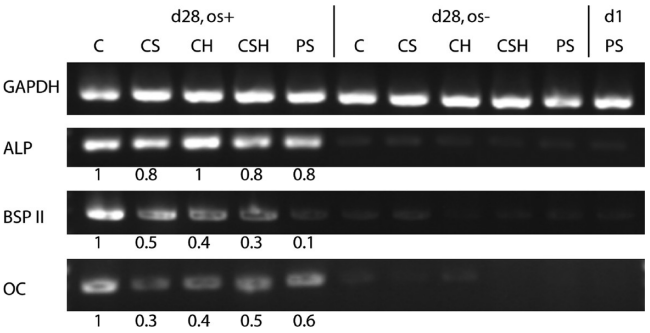

Figure 4. RT-PCR expression analysis of osteogenically induced hBMSC after 28 days of cultivation with osteogenic supplements (os+) or without osteogenic supplements (os−) on the different scaffold modifications. Gene expression intensities arranged in columns represent cells cultivated on collagen scaffolds without mineral (C), with 25% silica (CS), with 25% HAp (CH), with 12.5% silica +12.5% HAp (CSH), and on polystyrene (PS), respectively. Gene expression of hBMSC after 1 day on PS is illustrated as a reference. In the case of osteogenically induced cells, expression of the markers was normalized to the expression of the housekeeping gene GAPDH. For comparison, the highest values were set to 1.

collagen-HAp scaffolds (CH). Therefore, the cylindrical shape, necessary for measurement of confidable values for mechanical properties, was not guaranteed in these cases, and consequently no data is presented. However, the presence of 12.5 wt % silica (CSH) or 25 wt % silica (CS) resulted in stabilization, so that the scaffolds maintained their cylindrical shape during the cross-linking procedure and during immersion in PBS performed for determination of mechanical properties in the wet state. Typical stress-compression curves of CS and CSH determined for chemically cross-linked samples and PBS soaked scaffolds demonstrated highly elastic behavior of these scaffold modifications (Figure 2e, f).

3.3. Adhesion, Proliferation, And Differentiation of hBMSC. In vitro proliferation and differentiation analyses were performed to assess the effect of silica and HAp individually or combined on the scaffold's biocompatibility. Cell numbers detected after one day corresponded to about 85−95% of the seeded cell numbers indicating good initial adherence on each scaffold modification (Figure 3). Osteogenic induction from day 3 obviously was accompanied by slightly enhanced proliferation rates and cell numbers increased finally by factors of 4−6 during 28 days of cultivation. Comparing the scaffold modifications, the mineralization of collagen with silica, HAp or a combination of both had no significant effect on cell behavior. Relative ALP activity of the noninduced cell fractions remained at the base level for the whole cultivation time. The osteogenically induced cell fractions exhibited the typical maximum around day 14 on PS (control, data not shown) and around day 21 on the collagen scaffold (C) as well as on the collagen scaffold mineralized with 25 wt % HAp (CH). Interestingly, the values detected for relative ALP activity on silica-containing scaffolds were lower (CS os+ day 14 and day 21, CSH os+ day 14) compared to other scaffold modifications and were still increasing until day 28.

Gene expression analysis of osteogenically induced hBMSC after 28 days of cultivation (Figure 4) revealed an ALP transcript level that was highest on the scaffold with 25 wt % HAp. The values for the other scaffold modifications were similar. BSP II expression was much higher on the scaffolds compared to the PS control. However the transcript level of OC was lowest for collagen with 25 wt % silica. HBMSC cultivated for 1 day on PS as well as cells cultivated for 28 days on the scaffolds without addition of osteogenic supplements showed no expression of the mentioned markers.

Microscopic analysis was performed for qualitative evaluation of cell adhesion, proliferation, and differentiation. MTT staining one day after seeding confirmed well cell activity represented by dark color and predominantly located on the upper (cell-seeded) sides of the scaffolds (Figure 5a−d). The pure collagen scaffold seemed to provide best conditions for cell intrusion during the seeding procedure. The intense staining was observed throughout the whole cross-section in that case. Weaker and graded staining from the top to the bottom was detected for the mineralized modifications of the scaffolds. After 14 days of cultivation (Figure 5e−h), the intensity of the dark color increased on all scaffold modifications confirming the cell proliferation already determined by LDH activity analysis. Whereas the pure collagen scaffold suggested a very uniform distribution of cell activity, the peripheral areas of the mineralized scaffolds were clearly preferred. These results were confirmed by cLSM after 28 days of cultivation (Figure 5i−l). The cells maintained their adherence within the cultivation time and were capable to proliferate. Further cell proliferation resulted in uniform distribution of spread cells over the whole scaffold. Especially for the scaffold mineralized with 25 wt % silica (Figure 5 j) a lower cell

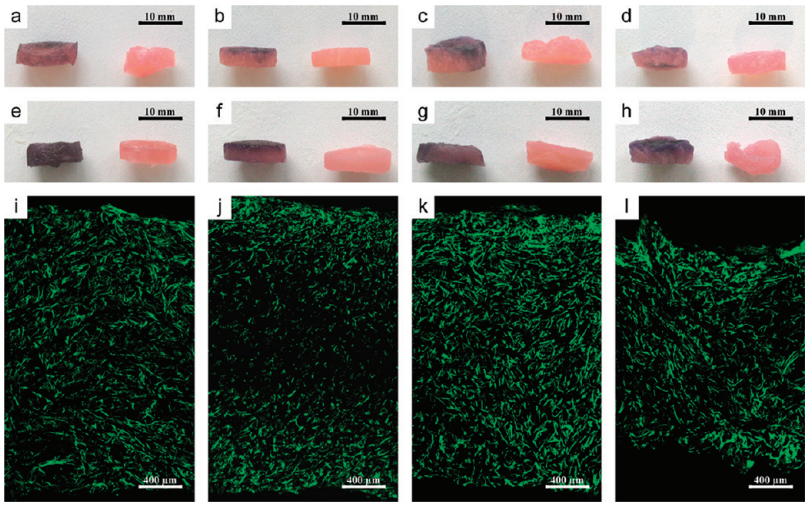

Figure 5. Photographs of MTT stained scaffold cross sections 1 day (left-hand side in a—d), 14 days after seeding (left-hand side in e—h), and control scaffolds without cells (right-hand side in a—h), respectively. Actin skeletons in the same cross sections after 28 days of cultivation are shown in the merged CLSM images (i—l). The columns represent the collagen scaffold (a, e, i) without mineral, (b, f, j) with 25% silica, (c, g, k) with 25% HAp, and (d, h, j) 12.5% silica and 12.5% HAp, respectively.

population in the inner area of the scaffold cross-section was observed.

Comparing cLSM images after 1 day and 28 days, cell proliferation was clearly recognized by enhanced lateral density of green visualized actin (Figure 6). ALP activity occurring as yellow aggregates was observed on all samples, confirming the biochemical and molecular-biological detection of that osteoblastic marker (Figure 6e—h). From these results, differences between the four scaffold modifications could not be defined.

4. DISCUSSION

Conventional mineralization techniques, such as plasma spraying, are inappropriate for samples containing organic components because of the high heat generation and inability to ensure homogeneous mineral distribution also inside the scaffolds.[25] The aim of the present study was to evaluate the combination of two mineralization methods for collagen scaffolds; silicification using the sol—gel method and embedding HAp particles by mixing at ambient conditions. The scaffolds were fabricated in groups containing silica, HAp, or equal shares of both, with the total amount of mineral kept constant at 25 wt %. The composite hydrogels obtained as an intermediate were freeze-dried, chemically cross-linked, and freeze-dried again. The resulting pore size was controlled by the rate of ice nucleation during the cooling process and consequent sublimation of ice crystals.[2] Because collagen concentration and cooling rate were kept constant in the present study, changes in resulting structural, mechanical, and biological properties were attributed to the mineral phases. The mean pore sizes observed for all scaffold modifications were similar to structures that were obtained when scaffolds based on biomimetically HAp-mineralized collagen were prepared.[26]

For scaffold modifications CS and CSH, silicic acid was present when collagen fibrils arranged to form fibers, surfaces, and finally pore walls of the scaffold. The interaction of silica species with amine groups of collagen has been shown to affect these processes.[18,23] Silica can envelop collagen fibers[19,23] or can act as a cross-linking spacer.[27] Previous studies also reported that silane is able to bridge gelatin chains resulting in hybrids, which is a system similar to the present one since gelatin is denatured collagen.[28] In the present study SEM imaging suggested silica to be homogeneously distributed in the collagen matrix. The effect that the presence of silicic acid causes separation of collagen fibrils is in clear agreement with previous results reported for hybrid silica-collagen hydrogels.[29] In these cases, the samples were built up from entangled networks with overcrossing areas of ropelike twisted bundles of collagen fibrils, which were similar to those obtained in the present study. Furthermore, Eglin et al. reported that highly concentrated poly-(silicic acid) adsorbed locally on protein chains, hinders their association.[30]

In contrast, HAp added to the collagen suspension was finally embedded as particles/aggregates in the collagen matrix or in the silica/collagen matrix. The challenges of HAp dispersion in polymer matrices were reviewed by Supova.[31] Especially the incorporation of micrometer-sized mineral phases into collagen scaffolds can cause problems with resorbability and brittleness of resulting constructs.[32]

Considering the macroscopic properties of the scaffolds, polymerizing silica obviously acted as a cross-linker and densified the organic matrix, which is confirmed by the templating effect known for collagen[23,33] as well as slight shrinking of the scaffold observed during freeze-drying. Despite that apparent density of the scaffold was enhanced due to silicification, the stiffness in the dry state before chemical cross-linking was not improved. In contrast the significantly enhanced Young's modulus of scaffolds CH obviously was a result of the large calcium phosphate particles. At higher strain rates, the inorganic/organic ratio seems to be the dominant parameter over the nature of the mineral. As a result, silica and HAp as sole mineral phases or combined had similar effects on mechanical properties of the scaffolds. Chemical cross-links initiated by EDC/NHS are predominantly formed between carboxyl and amine groups of the adjacent collagen molecules of the scaffold matrix which usually results in increased mechanical properties.[34] It was not possible to obtain data for cross-linked dry or wet samples of C and CH since the scaffolds collapsed due to capillary forces exceeding the materials strength during the cross-linking procedure. In contrast, silicification

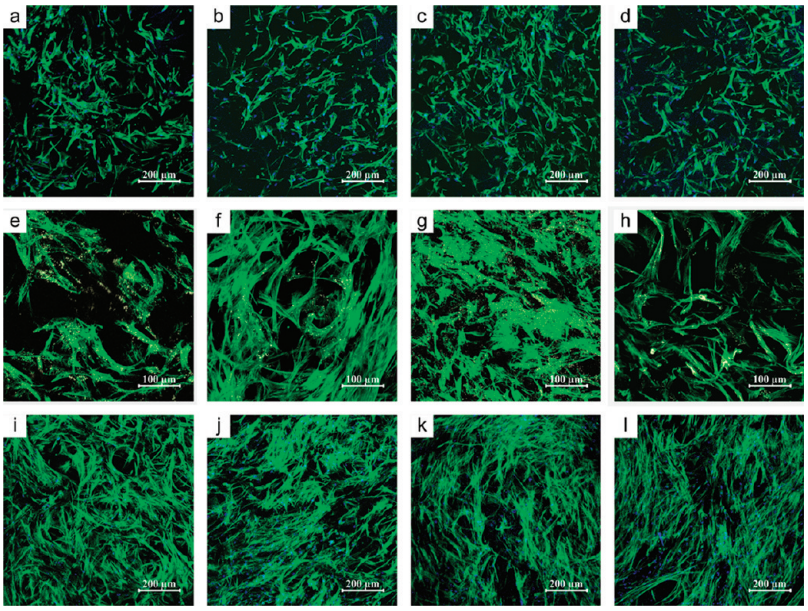

Figure 6. CLSM imaging of the cells on top of the scaffolds (a−d) one day after seeding, (e−h) 14 days after seeding, and (i−l) 28 days after seeding. In the first and third row cell nuclei are visualized blue and actin skeletons green. In the second row, actin skeletons (green) and ALP activity (yellow) are visualized at higher magnifications. The columns represent the collagen scaffold (a, e, i) without mineral, (b, f, j) with 25% silica, (c, g, k) with 25% HAp, and (d, h, j) 12.5% silica and 12.5% HAp, respectively.

performed for samples CS and CSH enhanced the scaffold's resistance against capillary forces and facilitated further characterization. The decrease in Young's moduli and compression strength of cross-linked CS as well as CSH in the dry state is attributed to imperfect chemical cross-linking and damaging of especially the silica network during the additional freeze-drying procedure. Considering the first point, previous results suggested that the amount of EDC/NHS initiated cross-links can be limited because of occupation of amine groups by silica which is also able to cross-link amine groups.[23] On the supposition that EDC/NHS cross-links and silica cross-links have similar strengths in the collagen matrix, the equal Young's moduli of modifications CS and CSH (half of the silica percentage compared to CS) in the dry state after cross-linking can be explained. However, it could also be possible that silica cross-links are fewer but stronger or more numerous but weaker. Although HAp mineralization had a strong influence on low-strain mechanical properties, high silica percentages showed advantages when compressive strength of CS and CSH after cross-linking and especially in the wet state is compared. In these cases, HAp addition did not compensate the corresponding amount of silica. Furthermore, cyclic loading of the scaffolds demonstrated creeping of the CS and CSH scaffolds.

Pore size distribution and corresponding specific surface area can affect initial cell adhesion which in turn can mediate all subsequent events such as proliferation, migration, and differentiation within the scaffold.[35,36] The commonly used Picogreen kit (Invitrogen) which is based on cell number determination by DNA measurement was not suitable in the present study due to DNA binding on the scaffold material. Therefore, LDH analysis, which measures the cell viability served the purpose without being disturbed by the scaffold material. One day after seeding similar cell numbers were determined by biochemical analysis for each scaffold modification, however MTT staining clearly revealed differences in initial cell distribution. Especially collagen silicification seems to limit cell migration capability compared to the other scaffold modifications. MTT staining is a valuable method for the visualization of viable cells in a large volume.[37] The reagent is incorporated by viable cells and is intracellularly transformed into an insoluble dark blue colored formazan derivative. MTT staining and cLSM imaging showed the widespread distribution of cells throughout the scaffolds. The images confirmed that the cells migrated to the center of the scaffolds. The poorer cell intrusion observed for the scaffolds with the highest silica concentration is attributed to morphological aspects of the pore structure. Obvious reasons are pore size distributions shifted to lower values or disturbed interconnectivity due to collagen bundles located in pore necks. LDH activity analysis and MTT staining revealed proliferation and viability of the cells over the whole cultivation time of 28 days. These results correspond with previous studies carried out with varied seeding conditions on collagen scaffolds mineralized with HAp.[38]

Although it was reported that cell differentiation occurs at an expense of proliferation rate, in the present study the values for both osteogenically induced and negative control cell fractions were similar on each scaffold modifications. Some studies also report enhanced proliferation rates due to osteogenic induction which is attributed to the stimulatory effect of dexamethasone.[39,40] The ALP activity passing a typical maximum for the samples C and CH, characterizes cell mineralization at a late stadium of differentiation. The involved processes − especially adhesion and differentiation − are supported by RGD sequences being part of the collagen of the scaffolds which are recognized by the cells.[41] As a result, ALP activity as well as osteocalcin expression can enhance.[42,43] Obviously, enveloping the collagen fibrils with silica and subsequently covering the RGD peptides, caused prolonged ALP activity increase periods and probably a shift of the ALP maxima to later time points for cells cultivated on CS or CSH. Furthermore these effects can explain the decreased osteocalcin expression on the mineralized scaffolds compared to the pure collagen scaffolds. This is confirmed by the BSP II results showing the same trends.

Although the presence of silica in the scaffolds resulted in moderate effects on cell behavior, the fact that silica has been identified as an alternative mineralizing agent that can substitute HAp is of even higher relevance. Because silica instead of HAp will determine the strength of the scaffold, it will be possible to separate the mechanical properties of a scaffold from the HAp content. That enables the use of calcium phosphate phases like HAp predominantly or even solely as an agent that controls the calcium ion concentration around the scaffold. This is an important point of recent biomaterials development, since it becomes obvious that solid calcium phosphate phases can exhibit adverse effects on cell behavior due to their high bioactivity and the resulting calcium depletion when incubated in physiological medium, especially in SBF. In this context, Malafaya and Reis coined the phrase "calcium phosphate cytotoxicity".[44] Furthermore, different extracellular calcium ion concentrations are able to manipulate the osteogenic differentiation.[45] It is assumed that calcium ions, most likely acting through the calcium sensing receptors, are a key regulator of osteoblast cell fate.[46] A comparably high calcium ion concentration stimulates migration, proliferation, and differentiation of osteoblasts for bone formation.[47] On the other hand, increased extracellular calcium ion concentrations trigger the inhibition of bone resorption through osteoclast dysfunction and apoptosis.[48] Subsequently, the extracellular calcium concentration is able to interfere in the cross-talk between osteoblasts and osteoclasts and to manipulate the ratio of both cell types. In order to take advantage from this fact, it is necessary to adjust the extracellular calcium concentration in the close vicinity of the biomaterial.

CONCLUSION

The present study has demonstrated the mechanical reinforcement of collagen by constant ratios of 25 wt % silica or HAp as well as equal amounts of both mineral phases combined. Polymerizing silicic acid influenced collagen surface formation, acted as a cross-linker for collagen fibrils, and therefore may be applied instead of conventional chemical cross-linking. The effects of sol−gel silica and powdered HAp mineralization on the scaffold's mechanical properties are partially comparable and can be combined. Cell culture experiments demonstrated that the high biological activity of the collagen scaffolds is in principle maintained following addition of silica or/and HAp. However, silica was recognized to retard the osteogenic differentiation of hBMSC. Although the results indicate that mineralization can constrain cell intrusion, tailoring the scaffold's mechanical properties is possible by simultaneously maintaining biological performance of these scaffolds. Instead of the common use of calcium phosphates as structure forming substances, the reported "silica approach" will enable to use calcium phosphate phases exclusively as an active agent in order to control the bioactivity of biomaterials.

AUTHOR INFORMATION

Corresponding Author

*E-mail: sascha.heinemann@tu-dresden.de. Tel: +49 351 463 39381. Fax: +49 351 463 39401.

ACKNOWLEDGMENT

We gratefully acknowledge the financial support from Deutsche Forschungsgemeinschaft (DFG Collaborative Research Centre TRR 79/SP M3).

REFERENCES

(1) Heinemann, C.; Heinemann, S.; Worch, H.; Hanke, T. *Eur. Cell. Mater.* **2011**, *21*, 80–93.
(2) O'Brien, F. J.; Harley, B. A.; Yannas, I. V.; Gibson, L. *Biomaterials* **2004**, *25* (6), 1077–86.
(3) Heinemann, C.; Heinemann, S.; Bernhardt, A.; Lode, A.; Worch, H.; Hanke, T. *Eur. Cell. Mater.* **2010**, *19*, 96–106.
(4) Harley, B. A.; Leung, J. H.; Silva, E. C.; Gibson, L. J. *Acta Biomater.* **2007**, *3* (4), 463–74.
(5) Murugan, R.; Ramakrishna, S. *Compos. Sci. Technol.* **2005**, *65*, 2385–406.
(6) Kickelbick, G., Introduction to Hybrid Materials. In *Hybrid Materials. Synthesis, Characterization, and Applications*; Kickelbick, G., Ed.; Wiley-VCH: Weinheim, Germany, 2007; pp 1−48.
(7) Chan, C. K.; Kumar, T. S.; Liao, S.; Murugan, R.; Ngiam, M.; Ramakrishnan, S. *Nanomedicine* **2006**, *1* (2), 177–88.
(8) Watari, F.; Yokoyama, A.; Gelinsky, M.; Pompe, W., Conversion of functions by nanosizing - from osteoconductivity to bone substitutional properties in apatite. In *Interface Oral Health Science 2007*; Watanabe, M.; Okuno, O., Eds.; Springer Japan: Tokyo, 2008; pp 139−147.
(9) Boccaccini, A. R.; Erol, M.; Stark, W. J.; Mohn, D.; Hong, Z.; Mano, J. F. *Compos. Sci. Technol.* **2010**, *70* (13), 1764–76.
(10) Wahl, D. A.; Czernuszka, J. T. *Eur. Cell. Mater.* **2006**, *11*, 43–56.
(11) Ehrlich, H.; Deutzmann, R.; Brunner, E.; Cappellini, E.; Koon, H.; Solazzo, C.; Yang, Y.; Ashford, D.; Thomas-Oates, J.; Lubeck, M.; Baessmann, C.; Langrock, T.; Hoffmann, R.; Worheide, G.; Reitner, J.; Simon, P.; Tsurkan, M.; Ereskovsky, A. V.; Kurek, D.; Bazhenov, V. V.; Hunoldt, S.; Mertig, M.; Vyalikh, D. V.; Molodtsov, S. L.; Kummer, K.; Worch, H.; Smetacek, V.; Collins, M. J. *Nat. Chem.* **2010**, *2* (12), 1084–8.
(12) Carlisle, E. M. *Sci. Total Environ.* **1988**, *73* (1−2), 95–106.
(13) Schwarz, K., Significance and functions of silicon in warm-blooded animals: Review and outlook. In *Biochemistry of Silicon and Related Problems*; Bendz, G., Lindqvist, I., Eds.; Plenum Press: New York, 1978; pp 207−230.
(14) Seaborn, C. D.; Nielsen, F. H. *Biol. Trace Elem. Res.* **2002**, *89* (3), 251–61.
(15) Patwardhan, S. V. *Chem. Commun.* **2011**, *47* (27), 7567–82.
(16) Sakka, S. *J. Sol−Gel Sci. Technol.* **2008**, *46*, 241–9.
(17) Carturan, G.; Dal Toso, R.; Boninsegna, S.; Dal Monte, R. *J. Mater. Chem.* **2004**, *14*, 2087–98.
(18) Coradin, T.; Allouche, J.; Boissiere, M.; Livage, J. *Curr. Nanosci.* **2006**, *2* (3), 219–230.
(19) Ono, Y.; Kanekiyo, Y.; Inoue, K.; Hojo, J.; Nango, M.; Shinkai, S. *Chem. Lett.* **1999**, *6*, 475–6.
(20) Desimone, M. F.; Helary, C.; Rietveld, I. B.; Bataille, I.; Mosser, G.; Giraud-Guille, M. M.; Livage, J.; Coradin, T. *Acta Biomater.* **2010**, *6* (10), 3998–4004.
(21) Heinemann, S.; Heinemann, C.; Bernhardt, R.; Reinstorf, A.; Nies, B.; Meyer, M.; Worch, H.; Hanke, T. *Acta Biomater.* **2009**, *5* (6), 1979–90.
(22) Heinemann, S.; Coradin, T.; Worch, H.; Wiesmann, H.P.; Hanke, T. *Compos. Sci. Technol.* **2011**, *71* (16), 1873–80.
(23) Heinemann, S.; Ehrlich, H.; Knieb, C.; Hanke, T. *Int. J. Mater. Res.* **2007**, *98* (7), 603–8.
(24) Oswald, J.; Boxberger, S.; Jorgensen, B.; Feldmann, S.; Ehninger, G.; Bornhauser, M.; Werner, C. *Stem Cells* **2004**, *22* (3), 377–84.
(25) Lickorish, D.; Ramshaw, J. A.; Werkmeister, J. A.; Glattauer, V.; Howlett, C. R. *J. Biomed. Mater. Res., A* **2004**, *68* (1), 19–27.
(26) Bernhardt, A.; Lode, A.; Mietrach, C.; Hempel, U.; Hanke, T.; Gelinsky, M. *J. Biomed. Mater. Res., A* **2009**, *90* (3), 852–62.
(27) Patwardhan, S. V.; Clarson, S. J.; Perry, C. C. *Chem. Commun. (Camb.)* **2005**, No. 9, 1113–21.
(28) Ren, L.; Tsuru, K.; Hayakawa, S.; Osaka, A. *Biomaterials* **2002**, *23* (24), 4765–73.
(29) Desimone, M. F.; Helary, C.; Mosser, G.; Giraud-Guille, M.-M.; Livage, J.; Coradin, T. *J. Mater. Chem.* **2010**, *20*, 666–8.

(30) Eglin, D.; Shafran, K. L.; Livage, J.; Coradin, T.; Perry, C. C. *J. Mater. Chem.* **2006**, *16*, 4220–4230.
(31) Supova, M. *J. Mater. Sci. Mater. Med.* **2009**, *20* (6), 1201–13.
(32) Cunniffe, G. M.; Dickson, G. R.; Partap, S.; Stanton, K. T.; O'Brien, F. J. *J. Mater. Sci. Mater. Med.* **2010**, *21* (8), 2293–8.
(33) Patwardhan, S. V. *Chem. Commun.* **2011**, *47*, 7567–82.
(34) Sinz, A. *J. Mass Spectrom.* **2003**, *38* (12), 1225–37.
(35) Berry, C. C.; Campbell, G.; Spadiccino, A.; Robertson, M.; Curtis, A. S. *Biomaterials* **2004**, *25* (26), 5781–8.
(36) Anselme, K. *Biomaterials* **2000**, *21* (7), 667–81.
(37) Mauney, J. R.; Blumberg, J.; Pirun, M.; Volloch, V.; Vunjak-Novakovic, G.; Kaplan, D. L. *Tissue Eng.* **2004**, *10* (1−2), 81–92.
(38) Lode, A.; Bernhardt, A.; Gelinsky, M. *J. Tissue Eng. Regen. Med.* **2008**, *2* (7), 400–7.
(39) Jaiswal, N.; Haynesworth, S. E.; Caplan, A. I.; Bruder, S. P. *J. Cell. Biochem.* **1997**, *64* (2), 295–312.
(40) Beresford, J. N.; Joyner, C. J.; Devlin, C.; Triffitt, J. T. *Arch. Oral Biol.* **1994**, *39* (11), 941–7.
(41) Tirrell, M.; Kokkoli, E.; Biesalski, M. *Surf. Sci.* **2002**, *500*, 61–83.
(42) Yang, F.; Williams, C. G.; Wang, D. A.; Lee, H.; Manson, P. N.; Elisseeff, J. *Biomaterials* **2005**, *26* (30), 5991–8.
(43) Secchi, A. G.; Grigoriou, V.; Shapiro, I. M.; Cavalcanti-Adam, E. A.; Composto, R. J.; Ducheyne, P.; Adams, C. S. *J. Biomed. Mater. Res., A* **2007**, *83* (3), 577–84.
(44) Malafaya, P. B.; Reis, R. L. *Acta Biomater.* **2009**, *5* (2), 644–60.
(45) Nakamura, S.; Matsumoto, T.; Sasaki, J.; Egusa, H.; Lee, K. Y.; Nakano, T.; Sohmura, T.; Nakahira, A. *Tissue Eng., Part A* **2010**, *16* (8), 2467–73.
(46) Dvorak, M. M.; Siddiqua, A.; Ward, D. T.; Carter, D. H.; Dallas, S. L.; Nemeth, E. F.; Riccardi, D. *Proc. Natl. Acad. Sci. U. S. A.* **2004**, *101* (14), 5140–5.
(47) Yamaguchi, T. *J. Bone Miner. Metab.* **2008**, *26* (4), 301–11.
(48) Negishi-Koga, T.; Takayanagi, H. *Immunol. Rev.* **2009**, *231* (1), 241–56.